




## Experimental and computational studies of the binding properties of lower rim tetra- and di-substituted calix[4]arene amide derivatives with metal ions

Paula M. Marcos, Joel D. Fonseca, Carla S. Proença, José R. Ascenso, Raul J. Bernardino, Joanna Kulesza & Maria Bochenska

To cite this article: Paula M. Marcos, Joel D. Fonseca, Carla S. Proença, José R. Ascenso, Raul J. Bernardino, Joanna Kulesza & Maria Bochenska (2016): Experimental and computational studies of the binding properties of lower rim tetra- and di-substituted calix[4]arene amide derivatives with metal ions, *Supramolecular Chemistry*, DOI: [10.1080/10610278.2015.1093631](https://doi.org/10.1080/10610278.2015.1093631)



To link to this article: <http://dx.doi.org/10.1080/10610278.2015.1093631>

 View supplementary material 

 Published online: 06 Feb 2016.

 Submit your article to this journal 

 Article views: 11

 View related articles 

 View Crossmark data 

## Experimental and computational studies of the binding properties of lower rim tetra- and di-substituted calix[4]arene amide derivatives with metal ions

Paula M. Marcos<sup>a,b</sup>, Joel D. Fonseca<sup>a</sup>, Carla S. Proença<sup>a</sup>, José R. Ascenso<sup>c</sup>, Raul J. Bernardino<sup>d</sup>, Joanna Kulesza<sup>e</sup> and Maria Bochenska<sup>f</sup>

<sup>a</sup>Centro de Química Estrutural, Faculdade de Ciências da Universidade de Lisboa, Lisboa, Portugal; <sup>b</sup>Faculdade de Farmácia da Universidade de Lisboa, Lisboa, Portugal; <sup>c</sup>Centro de Química Estrutural, Instituto Superior Técnico, Lisboa, Portugal; <sup>d</sup>Laboratory of Separation and Reaction Engineering, ESTM, MARE Instituto Politécnico de Leiria, Peniche, Portugal; <sup>e</sup>Department of Fundamental Chemistry, Federal University of Pernambuco (UFPE), Recife, Brazil; <sup>f</sup>Department of Chemistry & Technology of Functional Materials, Gdansk University of Technology, Gdansk, Poland

### ABSTRACT

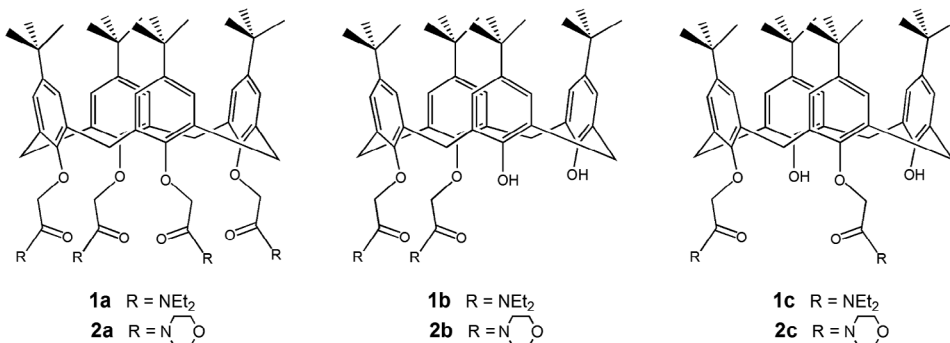
Experimental and theoretical binding studies of representative alkali, alkaline earth, transition, heavy metal and lanthanide cations by tetra- and di-substituted calix[4]arene amide derivatives (diethyl amide **1a–c** and morpholide amide **2a–c**) in the cone conformation were carried out. Binding was assessed by extraction experiments of the metal picrates from water to dichloromethane and proton NMR titrations. Density functional theory calculations were also performed to determine the binding energy of the complexes formed and to analyse the host–guest interaction modes. In the cases of ligands **1b** and **2c** with Na<sup>+</sup> and Ag<sup>+</sup> picrates, the extraction energy was also determined using the polarisable continuum model. The results are discussed in terms of the nature of the amide residue and the substitution pattern (1,3 vs. 1,2). Both tetra-amide derivatives are good extractants, showing preference for Na<sup>+</sup>, Ca<sup>2+</sup>, Ag<sup>+</sup> and Pb<sup>2+</sup> cations, mainly di-ethylamide **1a**. Concerning di-amide derivatives, the relative position of the substituents seems to be more important than the nature of the amide group in the extraction process. Proton NMR studies indicate the formation of 1:1 complexes between the amides and the cations studied, and DFT data show that all ligands form the most stable complexes with La<sup>3+</sup>.

### ARTICLE HISTORY

Received 3 August 2015  
Accepted 8 September 2015

### KEYWORDS

Calix[4]arene; tetra- and di-amide derivatives; metal cation binding; proton NMR titration; DFT



### Introduction

Calixarene-based molecules continue to be intensively investigated, mainly as ion and neutral molecule receptors in host–guest and supramolecular chemistry (1, 2). Although several calix[n]arene derivatives have been reported in the literature, calix[4]arenes have been the most studied compounds since David Gutsche optimised the synthesis of the parent compound *p*-*tert*-butylcalix[4]arene (3).

In particular, the ability of carbonyl-containing substituents on the lower rim of calix[4]arenes to bind metal ions

has been largely exploited (4–6). In this regard, functionalised calix[4]arenes with tertiary amide groups have been studied, both in solution and in the solid state, and have shown a high affinity for alkali, alkaline earth and some transition metal ions. Tetra(diethyl)amide derivative **1a** was the first and most studied tertiary amide (7–13). Other amide derivatives (14, 15) appeared later on, in order to determine the effects of the amide substituents on the efficiency and selectivity of the cation binding. Computational studies on metal ion binding by lower rim modified calix[4]arene derivatives have

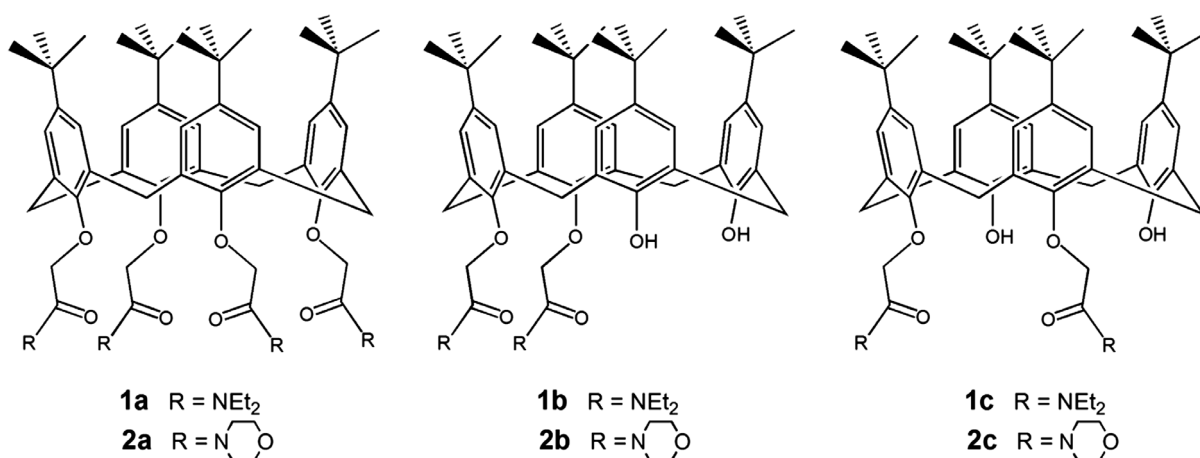


**Figure 1.** Structural formulae of calixarenes.

**Table 1.** Percentage extraction of alkali and alkaline earth metal picrates into  $\text{CH}_2\text{Cl}_2$  at 20 °C<sup>a</sup>.

	Li <sup>+</sup>	Na <sup>+</sup>	K <sup>+</sup>	Rb <sup>+</sup>	Cs <sup>+</sup>	Mg <sup>2+</sup>	Ca <sup>2+</sup>	Sr <sup>2+</sup>	Ba <sup>2+</sup>
l. radius <sup>b</sup> /Å	0.78	0.98	1.33	1.49	1.65	0.78	1.06	1.27	1.43
tetra-EtA ( <b>1a</b> ) <sup>c</sup>	63	96	74	24	12	9	98	86	74
tetra-MorphA ( <b>2a</b> )	—	71	23	—	—	10.5	48	16	19
1,2-di-EtA ( <b>1b</b> )	2.0	4.7	1.0	1.1	1.8	1.0	1.4	1.0	1.0
1,3-di-MorphA ( <b>2c</b> )	2.3	6.5	1.9	2.3	2.3	1.0	1.6	1.1	1.6

<sup>a</sup>Values with uncertainties less than 5%.

<sup>b</sup>V. M. Goldschmidt, *Skrifter Norske Videnskaps-Akad. Oslo, I, Mat.-Naturv. Kl.*, **1926**; data quoted in Y. Marcus, *Ion Properties*, Marcel Dekker, New York, **1997**, pp 46–47.

<sup>c</sup>Data taken from (8).

**Table 2.** Percentage extraction of transition and heavy metal picrates into  $\text{CH}_2\text{Cl}_2$  at 20 °C<sup>a</sup>.

	Mn <sup>2+</sup>	Fe <sup>2+</sup>	Co <sup>2+</sup>	Ni <sup>2+</sup>	Cu <sup>2+</sup>	Zn <sup>2+</sup>	Ag <sup>+</sup>	Cd <sup>2+</sup>	Pb <sup>2+</sup>
l. radius <sup>b</sup> /Å	0.83	0.78	0.75	0.69	0.73	0.75	1.15	0.95	1.18
tetra-EtA ( <b>1a</b> )	51	36	13	13	15	19	96	91	95
tetra-MorphA ( <b>2a</b> )	—	—	—	—	6.1	13.5	64	20	62
1,2-di-EtA ( <b>1b</b> )	0.5	3.1	0.5	1.1	1.0	2.1	1.0	1.0	1.5
1,3-di-MorphA ( <b>2c</b> )	1.0	—	—	—	1.5	2.5	3.1	2.1	3.1

<sup>a</sup>Values with uncertainties less than 5%.

<sup>b</sup>R. D. Shannon and C. T. Prewitt, *Acta Cryst.* **1969**, B25, 925; **1970**, B26, 1046; data quoted in Y. Marcus, *Ion Properties*, Marcel Dekker, New York, **1997**, pp 46–47.

also been reported (16). Molecular dynamics simulations were performed on calix[4]arene tetra-amide derivatives and some of their alkali and alkaline earth metal complexes (17–19). During the last years, computational tools have significantly improved, and more recently, density functional theory (DFT) studies have been extended to molecules as large as calixarenes (20–22).

Following our previous studies on cation-binding properties of calixarenes and homooxacalixarenes bearing amide functions at the lower rim (23–25), this study reports experimental and theoretical studies on the extraction and complexation properties of four lower rim tetra- and di-substituted calix[4]arene amide derivatives (**1a**, **2a** and **1b**, **2c**, respectively), in the cone conformation, towards a large variety of metal cations (alkali, alkaline earth, transition, heavy metal and lanthanides). Extraction experiments of metal picrates from an aqueous solution into dichloromethane and proton NMR titrations were performed. The structures and binding

energies of the complexes formed were investigated using DFT computational methods. These calculations were also extended to derivatives 1,3-diethylamide **1c** and 1,2-dimorpholide amide **2b** (Figure 1). Particular attention was given to the metals' preferred binding sites and to host–guest interaction modes. Also the extraction energy, from  $\text{H}_2\text{O}$  to  $\text{CH}_2\text{Cl}_2$ , was calculated in the cases of ligands **1b** and **2c** with sodium and silver picrates. To the best of our knowledge, no investigation using DFT has been conducted so far on the binding affinity of these di- and tetra-amide derivatives towards such a large variety of metal ions.

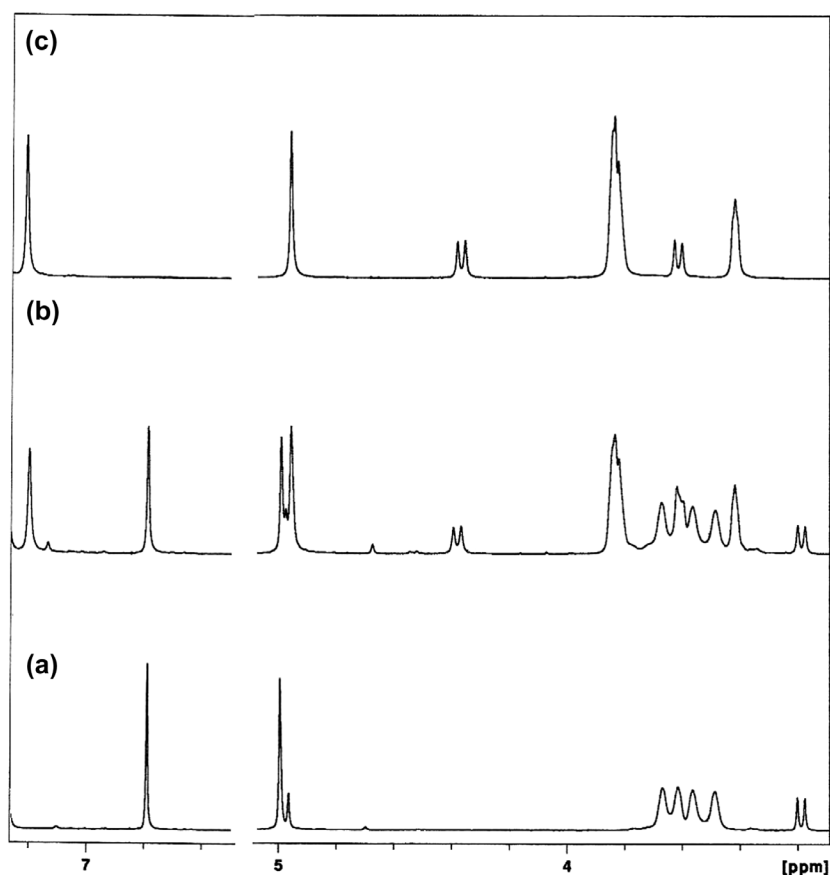
## Results and discussion

### Extraction studies

The ionophoric properties of the amide derivatives tetra-diethyl **1a**, tetra-morpholide **2a**, di-diethyl **1b** and di-morpholide **2c** (15) towards alkali, alkaline earth, transition,

**Table 3.** Percentage extraction of lanthanide picrates into  $\text{CH}_2\text{Cl}_2$  at 20 °C<sup>a</sup>.

	La <sup>3+</sup>	Ce <sup>3+</sup>	Pr <sup>3+</sup>	Nd <sup>3+</sup>	Sm <sup>3+</sup>	Eu <sup>3+</sup>	Gd <sup>3+</sup>	Dy <sup>3+</sup>	Er <sup>3+</sup>	Yb <sup>3+</sup>
l. radius <sup>b</sup> /Å	1.03	1.01	0.99	0.98	0.96	0.95	0.94	0.91	0.89	0.87
tetra-EtA ( <b>1a</b> ) <sup>c</sup>	12	14	17	19	23	24	20	23	18	18
tetra-MorphA ( <b>2a</b> )	8.2	9.4	8.4	10.5	11.1	11.4	9.6	10.8	9.2	9.0
1,2-di-EtA ( <b>1b</b> )	4.4	3.8	3.2	4.2	3.5	4.4	3.5	3.8	4.0	3.9
1,3-di-MorphA ( <b>2c</b> )	8.1	—	7.5	—	8.4	8.8	6.4	—	5.5	5.1

<sup>a</sup>Values with uncertainties less than 5%.<sup>b</sup>R. D. Shannon and C. T. Prewitt, *Acta Cryst.* **1969**, B25, 925; **1970**, B26, 1046; data quoted in Y. Marcus, *Ion Properties*, Marcel Dekker, New York, **1997**, pp 46–47.<sup>c</sup>Data taken from (25).**Figure 2.** 500 MHz <sup>1</sup>H NMR partial spectra of **2a** in  $\text{CDCl}_3/\text{CD}_3\text{OD}$  at 22 °C. (a) Free ligand, (b) upon addition of 0.5 and (c) 1 equiv of Pb perchlorate.

heavy metal and lanthanide metal cations were evaluated by the standard picrate extraction method (26). The results, expressed as a percentage of cation extracted (% *E*), are shown in Tables 1–3. Most of the data for derivative **1a** had already been obtained.

Concerning the tetra-substituted derivatives, the data reveal that diethylamide **1a** displays, in general, very high extraction levels for the alkali, alkaline earth and heavy metal cations, and moderate levels for the lanthanide ions. Towards transition metal cations,  $\text{Mn}^{2+}$  and  $\text{Fe}^{2+}$  are the best extracted cations, with percentages of 51 and 36%, respectively. Morpholide amide **2a**, although a weaker phase transfer agent,

shows a similar extraction profile to derivative **1a**. Morpholide **2a** displays a sharp peak selectivity for  $\text{Na}^+$  (71% *E*), a pronounced  $\text{Ca}^{2+}/\text{Mg}^{2+}$  selectivity and also a strong preference for the heavy cations  $\text{Ag}^+$  (64% *E*) and  $\text{Pb}^{2+}$  (62% *E*). In the case of the lanthanide ions, **2a** exhibits low extractability, but follows the same trend observed for **1a**, that is some preference for the middle lanthanides, such  $\text{Eu}^{3+}$  and  $\text{Sm}^{3+}$ . The lower efficiency in extraction of **2a** towards all the cations may be related with the higher rigidity of the morpholide group compared to the ethyl residue, making more difficult to undergo the conformational changes needed for the extraction process. This percentage decrease was more noticeable for

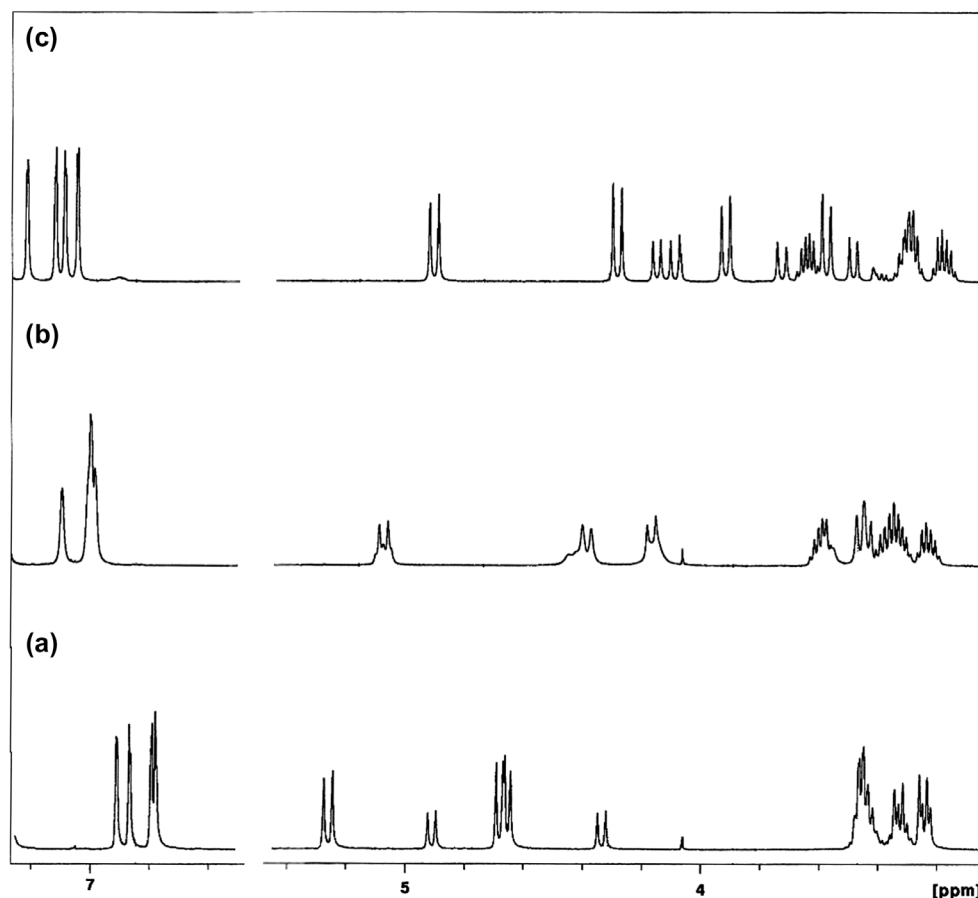


**Figure 3.** 500 MHz  $^1\text{H}$  NMR partial spectra of **1b** in  $\text{CDCl}_3/\text{CD}_3\text{OD}$  at 22 °C. (a) Free ligand, (b) upon addition of 0.5 and (c) 1 equiv of Ag triflate.

**Table 4.** Proton chemical shifts ( $\delta$ , ppm) of ligands **1a** and **2a** and their 1:1 metal complexes.

	t-Bu	ArCH <sub>2</sub> Ar			OCH <sub>2</sub> CO	ArH
		eq	ax	$\Delta\delta$		
<b>1a</b>	1.07	3.19	5.29	2.10	5.02	6.78
<b>1a</b> + Na <sup>+</sup>	1.19	3.33	4.46	1.13	4.53	7.16
<b>1a</b> + K <sup>+</sup>	1.17	3.32	4.61	1.28	4.62	7.15
<b>1a</b> + Ca <sup>2+</sup>	1.18	3.57	4.26	0.69	4.84	7.20
<b>1a</b> + Sr <sup>2+</sup>	1.17	3.60	4.31	0.71	4.83	7.22
<b>1a</b> + Ba <sup>2+</sup>	1.17	3.44	4.38	0.94	4.69	7.18
<b>1a</b> + Ag <sup>+</sup>	1.19	3.35	4.53	1.18	4.51	7.16
<b>1a</b> + Zn <sup>2+</sup>	1.16	3.43	4.36	0.93	4.83	7.12
<b>1a</b> + Pb <sup>2+</sup>	1.17	3.60	4.33	0.73	4.93	7.22
<b>1a</b> + La <sup>3+</sup>	1.19	3.79	4.30	0.51	5.34	7.34
<b>2a</b>	1.07	3.19	4.98	1.79	4.99	6.79
<b>2a</b> + Na <sup>+</sup>	1.17	3.39	4.51	1.12	4.70	7.15
<b>2a</b> + Ca <sup>2+</sup>	1.17	3.57	4.28	0.71	4.90	7.20
<b>2a</b> + Ag <sup>+</sup>	1.17	3.42	4.52	1.10	4.65	7.16
<b>2a</b> + Pb <sup>2+</sup>	1.16	3.61	4.36	0.75	4.95	7.21
<b>2a</b> + La <sup>3+</sup>	1.18	3.75	4.31	0.56	5.33	7.33

$\text{Cd}^{2+}$ ,  $\text{Sr}^{2+}$  and  $\text{K}^{+}$  cations. Similar results were observed before for pyrrolidine amide derivative (**8**). It was also reported that the presence of substituents containing cyclic structures decreases the extraction level of the cations (**14**).

Concerning the di-substituted derivatives, both amides are very weak extractants showing similar trends. The

carbonyl and phenoxy oxygen atoms of the two pendant arms should not be enough to surround the cations efficiently. Derivatives **1b** and **2c** display a very slight preference for  $\text{Na}^{+}$  and the highest percentages for the lanthanide ions. Although 1,3-di-morpholide amide **2c** is only marginally a better phase transfer agent than 1,2-diethyl amide **1b**, this behaviour was not expected. As it was previously seen, diethylamide is a better donor than morpholide amide. Thus, the substitution pattern (1,3 vs. 1,2) may account for these differences.

In order to gain some insight over the extraction process, theoretical simulations were performed using the polarisable continuum model (PCM) with the Los Alamos National Laboratory 2 double-zeta with the effective core potentials (LANL2DZ-ECP) basis set (**27**). The calixarene–cation affinity is observed when the free host molecule solubilised in dichloromethane is capable of removing the ion pair, cation and picrate anion, from the water phase into the organic phase. The stabilising energy resulting from the overall process was calculated for ligands **1b** and **2c** and sodium and silver picrates, representatives of two metal cation series. The results for  $\text{Na}^{+}$  were  $-24.10$  and  $-46.04$   $\text{kJ mol}^{-1}$  for **1b** and **2c**, respectively, while for  $\text{Ag}^{+}$  were  $-18.73$  and  $-15.23$   $\text{kJ mol}^{-1}$ .

**Table 5.** Proton chemical shifts ( $\delta$ , ppm) of ligands **1b** and **2c** and their 1:1 metal complexes.

	t-Bu	ArCH <sub>2</sub> Ar		OCH <sub>2</sub> CO	ArH
		eq	ax		
<b>1b</b>	1.01, 1.16	3.23, 3.24, 3.32	4.33, 4.66, 4.90	4.67, 5.25	6.77, 6.79, 6.86, 6.90
<b>1b</b> + Na <sup>+</sup>	1.06, 1.18	3.34, 3.39, 3.43	4.28, 4.22, 4.35	4.57, 4.83	6.91, 6.94, 6.96, 6.99
<b>1b</b> + K <sup>+</sup>	1.03, 1.17	3.27, 3.28, 3.36	4.31, 4.50, 4.75	4.59, 5.19	6.84, 6.86, 6.90, 6.94
<b>1b</b> + Ca <sup>2+</sup>	1.12, 1.20	3.41, 3.48, 3.63	4.26, 4.03, 4.46	4.43, 5.32	6.96, 7.03, 7.14
<b>1b</b> + Sr <sup>2+</sup>	1.03, 1.19	3.35, 3.41, 3.49	4.26, 4.08, 4.47	4.43, 5.16	6.86, 6.93, 6.97
<b>1b</b> + Ba <sup>2+</sup>	1.02, 1.17	3.25, 3.26, 3.35	4.32, 4.61, 4.87	4.66, 5.22	6.82, 6.88, 6.93
<b>1b</b> + Ag <sup>+</sup>	1.18, 1.27	3.48, 3.58, 3.73	4.09, 3.92, 4.15	4.28, 4.90	7.04, 7.09, 7.12, 7.21
<b>1b</b> + Zn <sup>2+</sup>	1.02, 1.17	3.26, 3.26, 3.35	4.30, 4.59, 4.79	4.64, 5.23	6.82, 6.89, 6.93
<b>1b</b> + Pb <sup>2+</sup>	1.19, 1.26	3.40, 3.66, 3.66	3.95, 4.08, 4.48	4.63, 5.32	7.07, 7.08, 7.10, 7.24
<b>1b</b> + La <sup>3+</sup>	1.04, 1.18	3.28, 3.29, 3.41	4.27, 4.43, 4.66	4.58, 5.24	6.85, 6.89, 6.92, 6.96
<b>2c</b>	0.94, 1.26	3.32	4.32	4.73	6.77, 7.01
<b>2c</b> + Na <sup>+</sup>	0.90, 1.29	3.39	4.17	4.81	6.78, 7.08
<b>2c</b> + Ca <sup>2+</sup>	0.93, 1.31	3.46	4.21	4.90	6.81, 7.14
<b>2c</b> + Ag <sup>+</sup>	1.05, 1.34	3.58	3.97	4.71	6.99, 7.21
<b>2c</b> + Pb <sup>2+</sup>	0.82, 1.32	3.41	4.16	4.91	6.65, 7.11
<b>2c</b> + La <sup>3+</sup>	0.87, 1.31	3.36	4.22	4.81	6.69, 7.11

Concerning the sodium cation, the best performance was observed with **2c**, in which the overall process was exothermic and almost the double of **1b**. In the case of the silver cation, the values obtained were very similar with **1b** being marginally better by  $\approx 3$  kJ mol<sup>-1</sup>. The results obtained in the former case agree with the experimental extraction data as can be seen in Table 1, while in the latter case, the opposite is observed, even though by a very small difference. Thus, the substitution pattern seems to be more relevant in the extraction process than the nature of the amide group.

### NMR binding studies

To obtain information on the cation-binding behaviour of derivatives **1a**, **1b**, **2a** and **2c**, specifically concerning the binding sites, proton NMR titrations were performed in CDCl<sub>3</sub>/CD<sub>3</sub>OD with these ligands and selected representatives of the alkali, alkaline earth, transition, heavy metal and lanthanide cation series (Na<sup>+</sup>, K<sup>+</sup>, Ca<sup>2+</sup>, Sr<sup>2+</sup>, Ba<sup>2+</sup>, Zn<sup>2+</sup>, Ag<sup>+</sup>, Pb<sup>2+</sup> and La<sup>3+</sup>).

Two different situations were found after the addition of the salts to the ligands. In the case of tetra-substituted derivatives, both amides (**1a** and **2a**) exhibit similar behaviours towards the cations. These titrations show that with [salt]/[ligand] ratios lower than one, both signals of the complexed and uncomplexed ligands are present in the spectra, indicating

that on the NMR time scale, the exchange rate between the two species is slow at room temperature. This behaviour reflects a high affinity of these ligands towards those cations. Upon reaching 1:1 ratios, all the signals for the free ligands disappear and those of the complexed ligands remain unaltered after subsequent addition of the salt, indicating a 1:1 metal-to-ligand stoichiometry (Figure 2). Small differences can, however, be observed in the case of Zn<sup>2+</sup> and La<sup>3+</sup> (with tetra-morpholide **2a**) spectra. With 0.5 equiv of added salts, the signals of both species were somewhat broad, becoming sharp after one equiv. In contrast, titrations of di-substituted derivatives (**1b** and **2c**) with all the cations initially induce some broadening of the signals (more noticed for 1,2-di-Et-amide **1b**) until the [salt]/[ligand] ratio reaches the unity, when the signals become sharp (Figure 3). This indicates a fast exchange rate between the two species on the NMR time scale, at room temperature, and consequently a weak affinity of these ligands towards the cations. Again, the NMR titrations suggest a 1:1 metal-to-ligand stoichiometry, since no further spectral changes were observed after subsequent additions of the salts.

Proton NMR data of the free and complexed ligands are shown in Tables 4 and 5. Complexation of the cations affects all the proton chemical shifts in the ligands. Tetra-Et-amide **1a** exhibits slightly larger variations than tetra-morpholide **2a**,

**Table 6.** Complexation energies  $\Delta E_c$  (kcal mol<sup>-1</sup>)<sup>a</sup> for the systems studied.

B3LYP/3-21G <sup>b</sup>	Na <sup>+</sup>	K <sup>+</sup>	Ca <sup>2+</sup>	Sr <sup>2+</sup>	Zn <sup>2+</sup>	Ag <sup>+</sup>	Pb <sup>2+</sup>	La <sup>3+</sup>
tetra-EtA ( <b>1a</b> )	-158.38	-108.09	-351.93	-303.73	-503.38	-157.28	-331.85	-625.10
tetra-MorphA ( <b>2a</b> )	-156.02	-96.03	-308.42	-262.90	-509.18	-144.62	-310.31	-612.02
1,2-di-EtA ( <b>1b</b> )	-141.65	-84.06	-300.30	-251.26	-480.69	-137.84	-283.28	-534.49
1,2-di-MorphA ( <b>2b</b> )	-118.15	—	-277.00	—	—	-125.37	-270.19	-512.83
1,3-di-EtA ( <b>1c</b> )	-129.75	—	-269.73	—	—	-134.68	-283.23	-536.61
1,3-di-MorphA ( <b>2c</b> )	-130.06	-76.12	-284.96	-236.29	-476.47	-131.62	-275.56	-525.58

<sup>a</sup> $\Delta E_c$  corresponds to the process  $L + M^{n+} \rightarrow [L - M^{n+}]$ , where L represents each of the ligands and M<sup>n+</sup> represents each one of the cations.

<sup>b</sup>Geometry optimisations were carried out at the referred level of theory for all the structures, except for Pb<sup>2+</sup> and La<sup>3+</sup> structures, where the LANL2DZ-ECP basis set was used, as implemented in Gaussian 03.

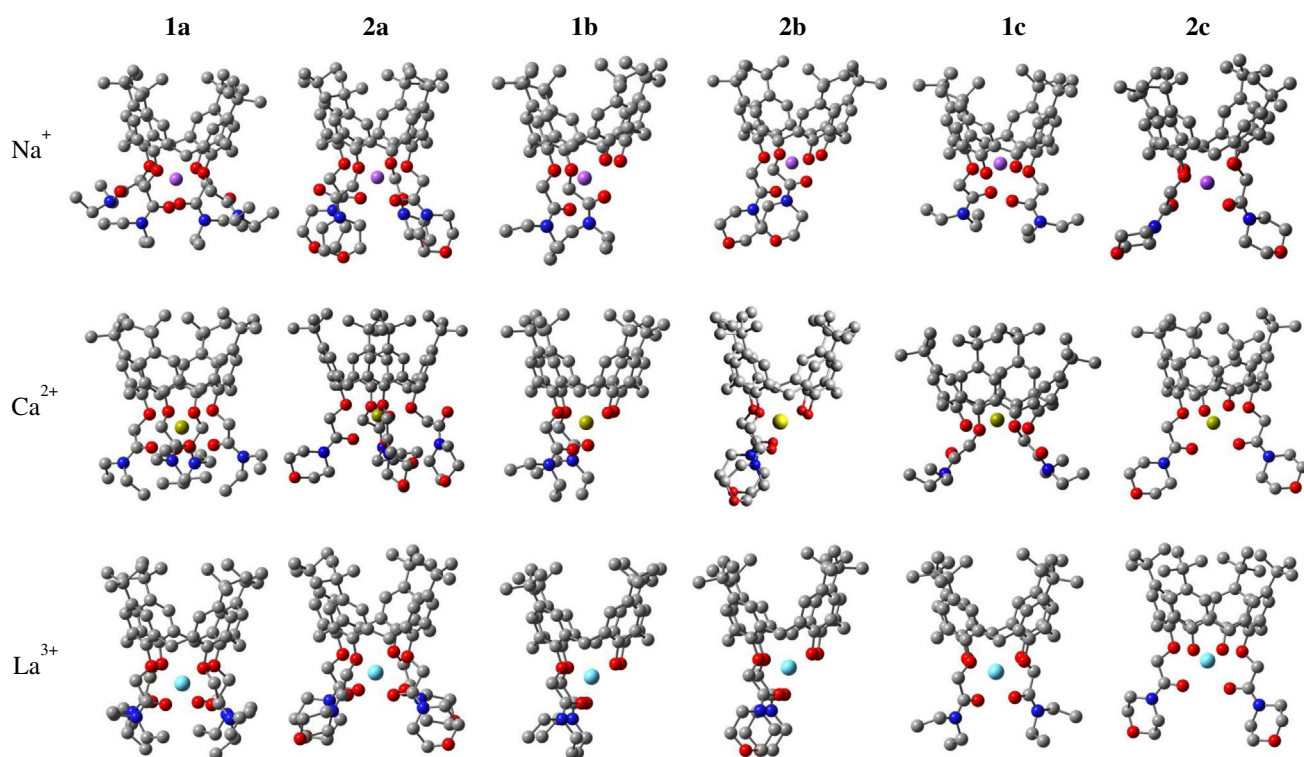


**Figure 4.** (Colour online) Optimised structures for the  $\text{Na}^+$  (upper row),  $\text{Ca}^{2+}$  (middle row) and  $\text{La}^{3+}$  (bottom row) complexes with the ligands studied. All the hydrogen atoms were removed for clarity.

**Table 7.** Selected distances (in Å) for  $\text{Na}^+$ ,  $\text{Ca}^{2+}$  and  $\text{La}^{3+}$  complexes with all the ligands studied.

	$\text{Na}^+$		$\text{Ca}^{2+}$		$\text{La}^{3+}$	
	$\text{O}_{\text{phen}}\text{-metal}^{\text{a}}$	$\text{O}_{\text{carb}}\text{-metal}^{\text{b}}$	$\text{O}_{\text{phen}}\text{-metal}^{\text{a}}$	$\text{O}_{\text{carb}}\text{-metal}^{\text{b}}$	$\text{O}_{\text{phen}}\text{-metal}^{\text{a}}$	$\text{O}_{\text{carb}}\text{-metal}^{\text{b}}$
<b>1a</b>	2.27, 2.30 2.28, 2.30	2.31, 2.31 3.80, 3.81	2.45, 2.46 2.46, 2.45	2.44, 2.46 2.44, 2.46	2.63, 2.63 2.63, 2.63	2.49, 2.50 2.50, 2.49
<b>2a</b>	2.31, 2.29 2.52, 3.32	2.37, 2.49 2.86, 4.25	2.38, 2.38 2.41, 2.41	2.38, 2.43 4.87, 4.94	2.63, 2.63 2.62, 2.63	2.50, 2.50 2.50, 2.50
<b>1b</b>	2.24, 2.60 2.15, 2.19	2.25 2.51	2.35, 2.33 2.36, 2.37	2.33 2.38	2.51, 2.49 2.49, 2.51	2.41 2.41
<b>2b</b>	2.18, 2.25 2.17, 2.25	2.26 2.87	2.35, 2.33 2.37, 2.36	2.33 2.38	2.49, 2.50 2.49, 2.50	2.41 2.41
<b>1c</b>	2.20, 2.16 2.17, 2.22	3.65 3.69	2.34, 2.24 2.24, 2.34	3.75 3.75	2.53, 2.47 2.47, 2.53	2.40 2.40
<b>2c</b>	2.66, 2.19 2.17, 2.21	2.18 2.60	2.66, 2.32 2.30, 2.33	2.31 2.33	2.53, 2.48 2.48, 2.53	2.40 2.40

<sup>a</sup>Distances between the cation and the oxygen atoms of the phenoxy groups ( $\text{O}_{\text{phen}}$ ).

<sup>b</sup>Distances between the cation and the oxygen atoms of the carbonyl groups ( $\text{O}_{\text{carb}}$ ).

but both follow the same trends (Table 4). The largest chemical shift changes are recorded for the aromatic protons and the bridging equatorial methylene protons ( $\text{ArCH}_2\text{Ar}$ ), which move downfield, and by the bridge axial methylene protons and the methylene protons of the  $\text{OCH}_2\text{CO}$  group (except for  $\text{La}^{3+}$ ), which move upfield. It has been observed that the shift variations of the methylene protons of the  $\text{OCH}_2\text{CO}$  groups in closely related dihomooxalix[4]arene amide derivatives (23, 25) are upfield for the monovalent cations and downfield for the divalent and trivalent cations. A closer examination of the spectral changes upon complexation indicates that these tetra-amides behave in a similar way. Divalent cations

still exhibit upfield shifts, but much smaller than the monovalent cations (for example,  $\Delta\delta = 0.34\text{--}0.29$  ppm for  $\text{M}^+$  and  $0.09\text{--}0.04$  ppm for  $\text{M}^{2+}$  in the case of **2a**), and  $\text{La}^{3+}$  shows a downfield shift of 0.34 ppm for **2a**. As observed for other calixarenes, the variation in chemical shift experienced by the equatorial methylene protons ( $\text{ArCH}_2\text{Ar}$ ) is downfield and smaller than that of the axial protons, but in the case of  $\text{La}^{3+}$  ( $\Delta\delta = 0.60$  and  $0.56$  ppm, respectively for **1a** and **2a**), it is still very high. Upon complexation, the differences in the chemical shifts between the axial and the equatorial protons of the  $\text{CH}_2$  bridges decrease in all cases, being closer to 0.90 ppm (28), mainly for  $\text{Zn}^{2+}$ ,  $\text{Ba}^{2+}$  and  $\text{Pb}^{2+}$  (both compounds). This

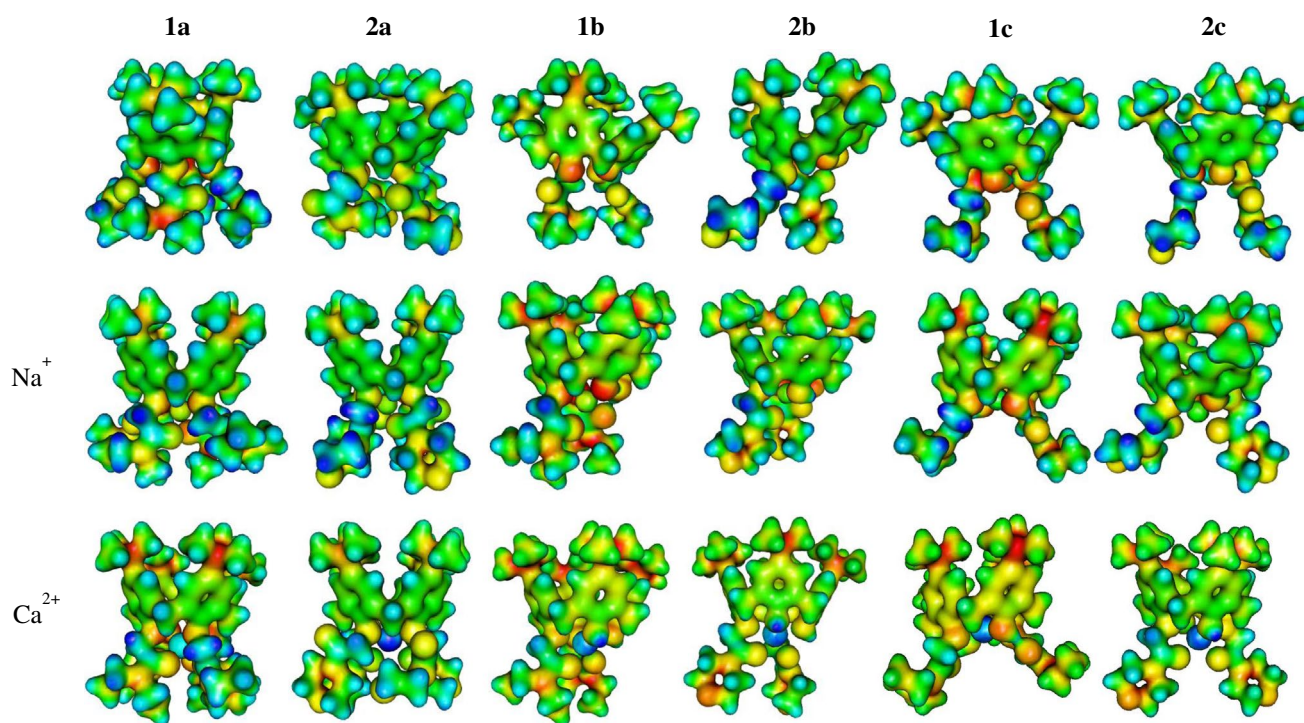


**Figure 5.** (Colour online) Electrostatic potential maps for the free ligands (upper row) and Na<sup>+</sup> (middle row) and Ca<sup>2+</sup> (bottom row) complexes. The electrostatic potential (in a.u.) is represented over a constant electronic isodensity  $\rho$  (in  $\text{\AA}^{-3}$ ) surfaces of volume  $V_s$  (in  $\text{\AA}^{-3}$ ). All figures correspond to  $\rho = 0.05 \text{\AA}^{-3}$  and the potential varies, for all ligands, from +0.30 (dark blue) to -0.25 (red) except for **1a** which varies from +0.90 to -0.50 for Na<sup>+</sup> and from +0.50 (dark blue) to -0.10 (red) for Ca<sup>2+</sup> complexes.

suggests that the free ligands depart from a distorted cone conformation and adopt a more regular cone conformation after complexation. The smallest variations are observed for the protons of the *tert*-butyl and substituent groups (diethyl and morpholide), and the multiplet of the N(CH<sub>2</sub>CH<sub>3</sub>)<sub>2</sub> residue splits in two after complexation.

The magnitude of the chemical shift variations for these tetra-substituted ligands follows the order: La<sup>3+</sup> > divalent cations > monovalent cations.

Concerning the di-substituted derivatives, both follow the same trends, although 1,2-di-Etamide **1b** displays larger chemical shift variations than 1,3-di-morpholide **2c**. The most pronounced upfield shifts are recorded for the bridging axial methylene protons, and the aromatic and bridge equatorial methylene protons undergo the largest downfield shifts. In the case of **1b**, the methylene protons of the OCH<sub>2</sub>CO groups undergo upfield variations, mainly for Ag<sup>+</sup> and Na<sup>+</sup>, and small downfield variations for Pb<sup>2+</sup> and Ca<sup>2+</sup>. In the case of **2c**, all the cations (except Ag<sup>+</sup>) display downfield variations, more pronounced for the divalent cations Pb<sup>2+</sup> and Ca<sup>2+</sup>. For these bidentate derivatives, the Ag<sup>+</sup> and Pb<sup>2+</sup> complexation induce the highest shift variations followed by Ca<sup>2+</sup>.

For both types of compounds (tetra- and di-substituted), the largest shift changes shown by the protons adjacent to the oxygen donor atoms can be explained in terms of variations of both shielding and deshielding effects of the

aromatic rings and carbonyl groups upon cation binding to those donor atoms. Therefore, this suggests that the cation must be inside the cavity defined by the phenoxy and carbonyl oxygen atoms and bound through metal–oxygen interactions.

### Computational binding studies

All the structures (ligands and complexes) were fully optimised without symmetry constraints using the B3LYP hybrid functional (29–31). Although the comparison between gas phase and condensed phase structures is not direct, all the structures were geometry optimised solvent free. They are therefore expected to correlate primarily with gas state complex geometries and not necessarily with NMR data, in which the solvent will influence the relative energies. However, they can give some insight into the key differences between the conformers under investigation (32).

The relative affinities of ligands **1a**, **2a**, **1b** and **2c** towards some representative cations (Na<sup>+</sup>, K<sup>+</sup>, Ca<sup>2+</sup>, Sr<sup>2+</sup>, Zn<sup>2+</sup>, Ag<sup>+</sup>, Pb<sup>2+</sup> and La<sup>3+</sup>) were determined by DFT methods. These calculations were also extended to derivatives 1,3-diethylamide (**1c**) and 1,2-dimorpholide amide (**2b**) to have a better understanding of the relative affinities of the di-substituted amides **1b** and **2c**. The complexation energies for all the systems studied are presented in Table 6 and some of the metal–ligand structures obtained are illustrated in Figure 4, while



the free ligands and remaining complexes are presented in the Supporting Information (Figures S1 and S2). The effect of complexation can be seen in Tables 7 and S1, where the distances between the cations and the oxygen atoms of both phenoxy and carbonyl groups are listed.

The energies calculated (Table 6) show that tetra-substituted ligands present the strongest interactions with all the cations. In the case of morpholide amide, the 1,3-di-substituted derivative is slightly preferred over the 1,2-di-substituted while the opposite preference is observed for diethyl amide (except in the case of  $\text{La}^{3+}$ ). In addition to the lower basicity of the carbonyl group attached to the morpholide residue compared to that of the ethyl moiety, the lower flexibility of the former substituent can introduce a higher conformational rigidity in the ligands that may contribute to their weaker complexation ability. The overall stability order obtained was related to the cation charge indicating, as expected, that electrostatic interactions are an important factor in ligand-cation affinity.

A more detailed analysis of the data shows that for the alkali and alkaline earth metal cations studied ( $\text{Na}^+$ ,  $\text{K}^+$ ,  $\text{Ca}^{2+}$ , and  $\text{Sr}^{2+}$ ), all have a higher affinity for tetra-ligand **1a** compared to the other ligands.  $\text{Na}^+$  and  $\text{Ca}^{2+}$  form the more stable complexes compared to  $\text{K}^+$  and  $\text{Sr}^{2+}$ , respectively, most likely due to the smaller ionic radii of the former. Moreover, the doubly charged cations exhibit significantly larger binding energies than the singly charged cations as expected, due to the higher charge to radius ratio. Concerning the symmetry of the complexes, ligand **1a** exhibits a more symmetrical structure with  $\text{Ca}^{2+}$  cation, which interacts almost equally with all the oxygen atoms. For the transition and heavy metal cations  $\text{Zn}^{2+}$ ,  $\text{Ag}^+$  and  $\text{Pb}^{2+}$ , zinc has the greatest affinity for all the ligands, followed by lead and silver, respectively. As with the other cations, ligand **1a** is preferred, except in the case of  $\text{Zn}^{2+}$  where ligand **2a** is slightly better by  $\approx 6$  kJ mol $^{-1}$ . All  $\text{Zn}^{2+}$  complex geometries are similar and very symmetrical, as can be observed in Table S1. Among all doubly charged cations studied,  $\text{Zn}^{2+}$  presents the highest charge to radius ratio, and this is probably responsible for the high negative complexation energies obtained (Table 6). Finally, the complexation energies clearly demonstrate that  $\text{La}^{3+}$  cation presents the strongest affinity with all the ligands studied. In these complexes, the cation interacts almost symmetrically with all the oxygen moieties present, as can be observed by the metal–oxygen distances listed in Tables 7 and S1, and illustrated in Figure 4.  $\text{La}^{3+}$  is preferably bound in the ligand lower rim closer to the carbonyl oxygen atoms, as observed in the structural representations and confirmed by the metal–oxygen distances, ranging from 2.40 to 2.50 Å.

To visualise the electrostatic equilibria in the different ligands and complexes, electrostatic potential maps were

calculated over an electronic isodensity surface of  $\rho = 0.05$  Å $^{-3}$ . These maps are shown in Figure 5 for the free ligands and their  $\text{Na}^+$  and  $\text{Ca}^{2+}$  complexes. In this Figure, the red regions are those of relatively lower or more negative electrostatic potential and the blue regions correspond to higher or more positive electrostatic potential. The greater positive charge on  $\text{Ca}^{2+}$  compared to  $\text{Na}^+$  is clearly evident by the deeper shade of blue for the former. These maps are also helpful concerning the cation position within the ligand molecule. For example, the sodium asymmetric position is observed by the effect caused on the hydrogen atoms, causing some of them to become more positive. For calcium, this effect is also observed, although the complex symmetry is generally higher.

These electrostatic potential maps can also give some information regarding the steric constraints and/or energy barriers related to the extraction process. For example, a more sterically hindered ligand implies an initial step of lower rim opening for the cation to go inside the cavity as can be observed in the free ligand **2a** and its complexes. This rim opening implies a bigger energy barrier and corroborates our previous observations.

## Conclusions

Extraction and complexation properties of six tetra- and di-substituted calix[4]arene amide derivatives were investigated experimentally and theoretically. These properties were determined by liquid–liquid extraction, proton NMR and DFT studies. The results obtained showed that both tetra-substituted ligands were the strongest binders for all the cations, diethylamide **1a** showing the highest percentage of extraction and the more negative complexation energies. The lower binding ability of morpholide amide **2a** should reflect either the electronic properties of its substituent group as well as its higher rigidity, compared to the ethyl substituent. Concerning the substitution pattern, the 1,3-morpholide **2c** is more efficient than the 1,2-derivative **2b**, while the opposite was observed for ethylamide derivatives (**1b** and **1c**). The complexation stability order was found to be related to cation charge,  $\text{La}^{3+}$  complexes being the most stables with all the ligands.

## Experimental

### Extraction studies

Ligand **1a** and ligands **2a**, **1b** and **2c** were prepared according to references 7 and 15, respectively.

After mutual saturation of the solvents, equal volumes (5 mL) of aqueous solutions of metal picrates ( $2.5 \times 10^{-4}$  M) and solutions of the calixarenes ( $2.5 \times 10^{-4}$  M) in  $\text{CH}_2\text{Cl}_2$  were vigorously shaken for 2 min and then thermostated in a

water bath with mechanical stirring at 20 °C overnight. After complete phase separation, the absorbance  $A$  of picrate ion in the aqueous phase was determined spectrophotometrically ( $\lambda_{\text{max}} = 354$  nm). For each cation–calixarene system, the absorbance measurements were repeated at least four times. Blank experiments without calixarene were run under the same conditions, yielding an absorbance  $A_0$ . The percentage of cation extracted was calculated as the ratio  $100 \times (A_0 - A)/A_0$ . The details of the metal picrate preparation have already been described (33).

### Proton NMR titrations

Several aliquots (up to 3 equiv) of the salt solutions (0.25 M) in  $\text{CD}_3\text{OD}$  were added to  $\text{CDCl}_3$  solutions ( $5 \times 10^{-3}$  M) of the ligands directly in the NMR tube. The salts used were Na and K thiocyanates, Ca, Sr, Ba and Pb perchlorates, and Zn, Ag and La triflates. The spectra were recorded on a Bruker Avance III 500 Spectrometer after each addition of the salts. The temperature of the NMR probe was kept constant at 22 °C.

### Theoretical methods

All the calixarene–metal complexes were analysed using computational DFT methods. All the structures were fully optimised without symmetry constraints using the Becke three-parameter hybrid functional combined with the Lee, Yang and Parr correlation functional (B3LYP) (29–31) along with the split valence double-zeta Pople basis set 3-21G, which is well known to produce accurate geometries. For  $\text{Pb}^{2+}$  and  $\text{La}^{3+}$  cations, where that basis set was not available, the LANL2DZ-ECP was used for every atom.

The methods used were those implemented in the Gaussian 03 software package (34) and Molekel software (35) and have been described elsewhere (32). The vibrational frequency calculations were performed at the same level of theory to check that all structures were at the global minima of the potential energy surface (denoted by an absence of negative vibrational frequencies) and to correct the computed energies for zero-point energies as well as translational, rotational and vibrational contributions to the enthalpy. All the figures and electrostatic potential surfaces were constructed using Molekel software (35).

For each of the six studied calix[4]arene amide derivatives, the initial cation position was thoroughly tested, starting inside or outside the receptor cavity. The relative binding energies ( $\Delta E_b$  corresponding to the process  $\text{Ligand} + \text{M}^{n+} \rightarrow [\text{Ligand}-\text{M}^{n+}]$ , where  $\text{M}^{n+}$  represents each one of the cations) were calculated as the energy difference at 298 K between the final energy of the complexes and the sum of the energies of the calixarene ligand and the cation in study respecting the same theoretical level (32).

For the extraction calculations, an approach incorporating effective core potentials was found to be very effective in reducing computational expense. The LANL2DZ basis set was used, and the solvent was defined within the PCM using the integral equation formalism variant (IEFPCM) in Gaussian 03. The extraction energy was estimated by the relative difference between the ion pair (sodium and silver picrates) in water, the free calixarene molecules (**1b** and **2c**) in  $\text{CH}_2\text{Cl}_2$  and the species calixarene/cation/anion in the same solvent.

### Supplemental material

Supplemental data for this article can be accessed online here: <http://dx.doi.org/10.1080/10610278.2015.1093631>

### References

- (1) Asfari, Z.; Böhmer, V.; Harrowfield, J.; Vicens, J., Eds.; *Calixarenes 2001*; Kluwer Academic Publishers: Dordrecht, **2001**.
- (2) Gutsche, C.D. In *Calixarenes: An Introduction*, 2nd ed.; The Royal Society of Chemistry: Cambridge, **2008**.
- (3) Gutsche, C.D.; Iqbal, M. *Org. Synth.* **1990**, *68*, 234–237.
- (4) McKervey, M.A.; Schwing-Weill, M.J.; F. Arnaud-Neu, F. Cation Binding by Calixarenes. In *Comprehensive Supramolecular Chemistry*; Lehn, J.M., Gokel, G.W., Eds.; Elsevier: Oxford, **1996**; pp 537–603.
- (5) Arnaud-Neu, F.; McKervey, M.A.; Schwing-Weill, M.J. In *Calixarenes 2001*; Asfari, Z., Böhmer, V., Harrowfield, J., Vicens, J., Eds.; Kluwer Academic Publishers: Dordrecht, **2001**; pp 385–406; Arnaud-Neu, F.; Schwing-Weill, M.J.; Dozol, J.-F. In *Calixarenes 2001*; Asfari, Z., Böhmer, V., Harrowfield, J., Vicens, J., Eds.; Kluwer Academic Publishers: Dordrecht, **2001**; pp 642–662.
- (6) Craven, B.S.; Donlon, D.F.; McGinley, J. *Coord. Chem. Rev.* **2009**, *253*, 893–962.
- (7) Arduini, A.; Ghidini, E.; Pochini, A.; Ungaro, R.; Andreotti, G.D.; Calestani, G.; Ugozzoli, F. *J. Inclusion Phenom.* **1988**, *6*, 119–134.
- (8) Arnaud-Neu, F.; Schwing-Weill, M.J.; Ziat, K.; Cremin, S.; Harris, S.J.; McKervey, M.A. *New J. Chem.* **1991**, *15*, 33–37.
- (9) Arnaud-Neu, F.; Fanni, S.; Guerra, L.; McGregor, W.; Ziat, K.; Schwing-Weill, M.J.; Barrett, G.; McKervey, M.A.; Marrs, D.; Seward, E.M. *J. Chem. Soc., Perkin Trans.* **1995**, *2*, 113–118.
- (10) Beer, P.D.; Drew, M.G.B.; Leeson, P.B.; Ogden, M.I. *J. Chem. Soc., Dalton Trans.* **1995**, 1273–1283.
- (11) Danil de Namor, A.F.; Baron, K.; Chahine, S.; Jafou, O. *J. Phys. Chem. A* **2004**, *108*, 1082–1089.
- (12) Ali, A.; Rao, C.P.; Guionneau, P. *J. Chem. Sci.* **2008**, *120*, 237–247.
- (13) Danil de Namor, A.F.; Matsufuji-Yasuda, T.T.; Zegarraf-Fernandez, K.; Webb, O.A.; El Gamouz, A. *Croat. Chim. Acta* **2013**, *86*, 1–19.
- (14) Arnaud-Neu, F.; Barrett, G.; Fanni, S.; Marrs, D.; McGregor, W.; McKervey, M.A.; Schwing-Weill, M.J.; Vetrogon, V.; Wechsler, S. *J. Chem. Soc., Perkin Trans.* **1995**, *2*, 453–461.
- (15) Bochenska, M.; Banach, R.; Zielinska, A.; Kravtsov, V.J. *Incl. Phenom. Macrocyclic Chem.* **2001**, *39*, 219–228.
- (16) Chinta, J.P.; Ramanujam, B.; Rao, C.P. *Coord. Chem. Rev.* **2012**, *256*, 2762–2794.

- (17) Varnek, A.; Wipff, G. *J. Phys. Chem.* **1993**, *97*, 10840–10848.
- (18) Arnaud-Neu, F.; Barbosa, S.; Berny, F.; Casnati, A.; Muzet, N.; Pinalli, A.; Ungaro, R.; Schwing-Weill, M.J.; Wipff, G. *J. Chem. Soc., Perkin Trans.* **1999**, *2*, 1727–1738.
- (19) Horvat, G.; Stilinovic, V.; Kaitner, B.; Frkanec, L.; Tomisic, V. *Inorg. Chem.* **2013**, *52*, 12702–12712.
- (20) Shamova, L.I.; Shamov, G.A.; Antipin, I.S.; Konovalov, A.I. *J. Phys. Chem. A* **2009**, *113*, 5691–5699.
- (21) Horvat, G.; Stilinovic, V.; Hrenar, T.; Kaitner, B.; Frkanec, L.; Tomisic, V. *Inorg. Chem.* **2012**, *51*, 6264–6278.
- (22) Boda, A.; Sheikh, M.A. *J. Phys. Chem. A* **2012**, *116*, 8615–8623.
- (23) Marcos, P.M.; Félix, S.; Ascenso, J.R.; Segurado, M.A.P.; Pereira, J.L.C.; Khazaeli-Parsa, P.; Hubscher-Bruder, V.; Arnaud-Neu, F. *New J. Chem.* **2004**, *28*, 748–755.
- (24) Marcos, P.M.; Ascenso, J.R.; Cragg, P.J. *Supramol. Chem.* **2007**, *19*, 199–206.
- (25) Marcos, P.M.; Ascenso, J.R.; Segurado, M.A.P.; Cragg, P.J.; Michel, S.; Hubscher-Bruder, V.; Arnaud-Neu, F. *Supramol. Chem.* **2011**, *23*, 93–101.
- (26) Pedersen, C. *J. Am. Chem. Soc.* **1970**, *92*, 391–394.
- (27) Peerannawar, S.R.; Gejji, S.P. *Comput. Theor. Chem.* **1015**, *2013*, 44–51.
- (28) Gutsche, C.D. *Calixarenes*; The Royal Society of Chemistry: Cambridge, **1989**.
- (29) Becke, A.D. *J. Chem. Phys.* **1993**, *98*, 5648–5652.
- (30) Becke, A.D. *Phys. Rev. A* **1998**, *38*, 3098–3100.
- (31) Lee, C.; Yang, W.; Parr, R.G. *Phys. Rev. B* **1988**, *37*, 785–789.
- (32) Marcos, P.M.; Teixeira, F.A.; Segurado, M.A.P.; Ascenso, J.R.; Bernardino, R.J.; Cragg, P.J.; Michel, S.; Hubscher-Bruder, V.; Arnaud-Neu, F. *J. Phys. Org. Chem.* **2013**, *26*, 295–305.
- (33) Marcos, P.M.; Ascenso, J.R.; Segurado, M.A.P.; Bernardino, R.J.; Cragg, P.J. *Tetrahedron* **2009**, *65*, 496–503.
- (34) Frisch, M.J.; Trucks, G.W.; Schlegel, H.B.; Scuseria, G.E.; Robb, M.A.; Cheeseman, J.R.; Montgomery, J.A. Jr.; Vreven, T.; Kudin, K.N.; Burant, J.C.; Millam, J.M.; Iyengar, S.S.; Tomasi, J.; Barone, V.; Mennucci, B.; Cossi, M.; Scalmani, G.; Rega, N.; Petersson, G.A.; Nakatsuji, H.; Hada, M.; Ehara, M.; Toyota, K.; Fukuda, R.; Hasegawa, J.; Ishida, M.; Nakajima, T.; Honda, Y.; Kitao, O.; Nakai, H.; Klene, M.; Li, X.; Knox, J.E.; Hratchian, H.P.; Cross, J.B.; Bakken, V.; Adamo, C.; Jaramillo, J.; Gomperts, R.; Stratmann, R.E.; Yazyev, O.; Austin, A.J.; Cammi, R.; Pomelli, C.; Ochterski, J.W.; Ayala, P.Y.; Morokuma, K.; Voth, G.A.; Salvador, P.; Dannenberg, J.J.; Zakrzewski, V.G.; Dapprich, S.; Daniels, A.D.; Strain, M.C.; Farkas, O.; Malick, D.K.; Rabuck, A.D.; Raghavachari, K.; Foresman, J.B.; Ortiz, J.V.; Cui, Q.; Baboul, A.G.; Clifford, S.; Cioslowski, J.; Stefanov, B.B.; Liu, G.; Liashenko, A.; Piskorz, P.; Komaromi, I.; Martin, R.L.; Fox, D.J.; Keith, T.; Al-Laham, M.A.; Peng, C.Y.; Nanayakkara, A.; Challacombe, M.; Gill, P.M.W.; Johnson, B.; Chen, W.; Wong, M.W.; Gonzalez, C.; Pople, J.A. *Gaussian 03, Revision C.02*; Gaussian, Inc.: Wallingford CT, **2004**.
- (35) Varetto, U., *Molekel 5.4*. <http://ugovaretto.github.io/molekel-wiki/pmwiki.php/Main/Citing.html>.